THE ASTROPHYSICAL JOURNAL, 466:750–756, 1996 August 1

A DEEP X-RAY IMAGE OF M33

KNOX S. LONG
Space Telescope Science Institute, 3700 San Martin Drive, Baltimore, MD 21218; long@stsci.edu
PHILIP A. CHARLES
Department of Astrophysics, Oxford University, Oxford OX1 3RH, UK; pac@astro.ox.ac.uk
WILLIAM P. BLAIR
Department of Physics and Astronomy, Johns Hopkins University, Baltimore, MD 21218; wpb@pha.jhu.edu
AND
SHAWN M. GORDON
Lawrence Berkeley National Laboratory, Building 50-232, 1 Cyclotron Road, Berkeley, CA 94720; sgordon@athena.lbl.gov
Received 1995 November 27; accepted 1996 February 27

ABSTRACT

A 50.4 ks *ROSAT* Position Sensitive Proportional Counter image of the nearby spiral galaxy M33 reveals 37 sources within 15′ of the nucleus brighter than 7×10^{35} ergs s^{-1}. There are at least 13 additional sources farther from the nucleus, most of which are likely to be associated with M33 as well. Most of the bright sources that had been detected with *Einstein* in the same region are still visible. The bulk of the sources in the galaxy are associated with Population I tracers. Several of the sources are time variable. There are 10 sources in the image that lie within 20″ of optically identified supernova remnants (SNRs) in M33. The spectra of these sources are soft compared with most other sources of comparable brightness, and therefore it is likely that most of these X-ray sources are SNRs. Based on the identification of sources in M33, it appears likely that *ROSAT* hardness ratios of this type can be used to separate SNRs and compact sources in other nearby normal galaxies as well. The northern and the southern spiral arms of M33 appear as diffuse features in the X-ray image. There is additional diffuse (or unresolved source) emission throughout the inner portions of M33. The diffuse emission is softer than the faint point sources and the SNRs in the survey, and is well fitted in terms of a bremsstrahlung spectrum with $kT \sim 0.4$ keV and $\log N_H \sim 20.6$.

Subject headings: galaxies: individual (M33) — supernova remnants — X-rays: galaxies — X-rays: ISM

1. INTRODUCTION

M33 is one of the two spiral galaxies nearest the Milky Way. Because of its proximity (720 kpc; de Vaucouleurs 1978), relatively low inclination angle (57°; Searle 1971), and well-defined open spiral arms, M33 is an ideal galaxy for studying the X-ray properties of late-type spiral galaxies, and, as a result, both the imaging proportional counter (IPC) and the high-resolution imager (HRI) studies of M33 were undertaken using the *Einstein Observatory* (Long et al. 1981; Markert & Rallis 1983; Trinchieri, Fabbiano, & Peres 1988). These studies revealed a dominant nuclear source, the brightest source in the Local Group with $L_X \sim 10^{39}$ ergs s^{-1}, and 14 other sources with $L_X \geq 10^{37}$ ergs s^{-1} that were likely to be associated with M33. Most of the discrete sources are thought to be compact X-ray binaries, including one that is known to be an eclipsing system with a 1.787 day period (Peres et al. 1989; Schulman et al. 1993, 1994).

Schulman & Bregman (1995) have recently discussed an initial survey of M33 with the HRI on board *ROSAT* (Trümper 1983). Here we describe a survey of M33 with the *ROSAT* Position Sensitive Proportional Counter (PSPC). The PSPC has somewhat greater sensitivity, especially to diffuse emission, much better spectral resolution, and a larger field of view than the HRI, but the HRI has better spatial resolution. Our observations were intended to inventory the point-source populations in M33 to significantly lower luminosities than was possible with *Einstein*, and to use the improved spectral and spatial resolution of the PSPC to characterize the diffuse soft X-ray emission from M33.

2. OBSERVATIONS

ROSAT is an X-ray telescope that, with the PSPC at the focal plane, has a field of view of 2° and images X-rays in the energy range 0.1–2.4 keV with a resolution $E/\Delta E \sim 2.4E^{-0.5}$, where E is the photon energy in keV. The angular resolution varies with off-axis angle but is ~20″ (FWHM) within 20′ of the optical axis, which contains most of the visible light of M33. A complete description of the PSPC has been provided by Pfeffermann et al. (1986). Problems and procedures associated with the analysis of extended sources with the *ROSAT* PSPC are discussed by Snowden et al. (1994, hereafter SMBM).

The *ROSAT* PSPC was pointed at the nucleus of M33 (R.A. = $1^h33^m50^s.8$, decl. = 30°39′36″.6 [J2000]) for a total of 50.4 ks. There were three blocks of observations, in 1991 July, 1992 August, and 1993 January. The first block, in which 29.1 ks of good data were obtained, occurred during the so-called "reduced pointing" mode. During this period, the nodding of the telescope, which is carried out in order to smooth out the effects of the window support mesh on source counting rates, was reduced. The other two observations, lasting 5.0 and 16.3 ks, respectively, were carried out under normal conditions.

Despite the fact that the nominal pointing positions were identical in all the observations, inspection of the images showed that the apparent positions of the bright (0.6 counts

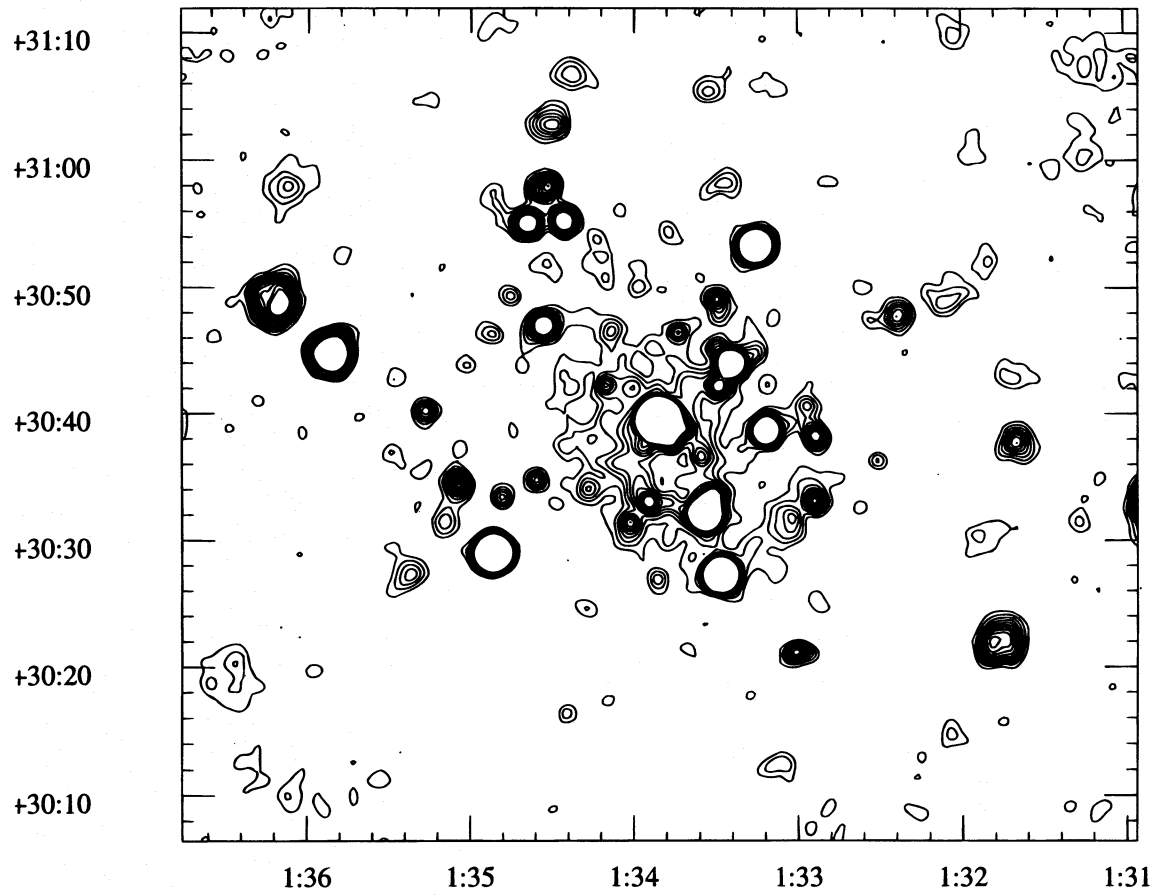

FIG. 1.—Contour plot of the 0.4–1.3 keV *ROSAT* PSPC image of M33. The image has been corrected for vignetting. The 10 contour levels range linearly from 0.48×10^{-3} to 1.6×10^{-3} s^{-1} arcmin^{-2}.

s^{-1}) nuclear source were changing from orbit to orbit, and especially from block to block of observing time. For example, taking the data from the three blocks of data separately, the declination of the bright nuclear source appeared to fall 6.″8 north, 11.″3 north, and 4.″8 south of the position of the nucleus of M33, which we took from deVaucouleurs & Leach (1981) to be $1^h33^m50^s.9$, 30°39′36.″8 (precessed to J2000). Therefore, we elected to recenter the nuclear X-ray source to the position of the optical nucleus of M33 for all the data. Using IRAF and the X-ray analysis tasks contained in PROS, we first calculated the offsets for each individual orbit from the peaks of the Gaussian-smoothed ($\sigma = 5''$) images of the nucleus. We then shifted and added the data from each orbit to form a new X-ray (".qp") image. As might be expected, the resulting X-ray image of the nucleus (and of other sources near the nucleus) is more symmetrical than the image resulting from a simple sum of the images. There is still a slight residual asymmetry in the appearance of the peak of the nuclear X-ray source, but this is attributable to small errors in our recentering process and higher order aspect problems in the standard reduction process; this is unimportant for the discussion that follows.

A contour plot of the X-ray image after correcting for vignetting is shown in Figure 1. The data include photons in the nominal energy range 0.4–1.3 keV (PI bins 41–131), and the vignetting function we used was obtained for the same range using the software package developed by Snowden (1994) to implement the SMBM analysis of diffuse emission. The central portion of the X-ray image superposed on an Hα CCD mosaic of M33 (Gordon et al. 1996) is shown in Figure 2 (Plate 17). There are evidently a large number of point sources dominated by the bright nuclear source that was observed with *Einstein*. From a comparison of the X-ray and Hα images of M33, it looks as if many of the sources in M33 are associated with H II regions in the galaxy. There appears to be unresolved emission throughout much of the galaxy and enhanced emission associated with both the southern and the northern spiral arms in M33.

3. ANALYSIS

3.1. *Point Sources*

The X-ray image from M33 is complex. The point-source response function for the PSPC varies over the visible image of M33, source confusion can affect sensitivity limits near bright sources, and regions of the galaxy were partially obscured by the PSPC rib structure. As a result, the identifications of point sources and measurements of their properties are not straightforward. We used the following procedure: Based on the standard data products and an inspection of the images, we identified a total of 59 potential point sources that were isolated from the effects of shadowing by the ribs. In order to evaluate the statistical significance of each source, we defined circular source regions with radii that varied from 25″ to 190″ depending on off-axis angle. We then defined a local background region, usually an annulus with any other source regions removed, and extracted the net pulse-height spectrum (with Gaussian errors) for each source candidate using the complete data set. Finally, we summed the spectra to determine the net

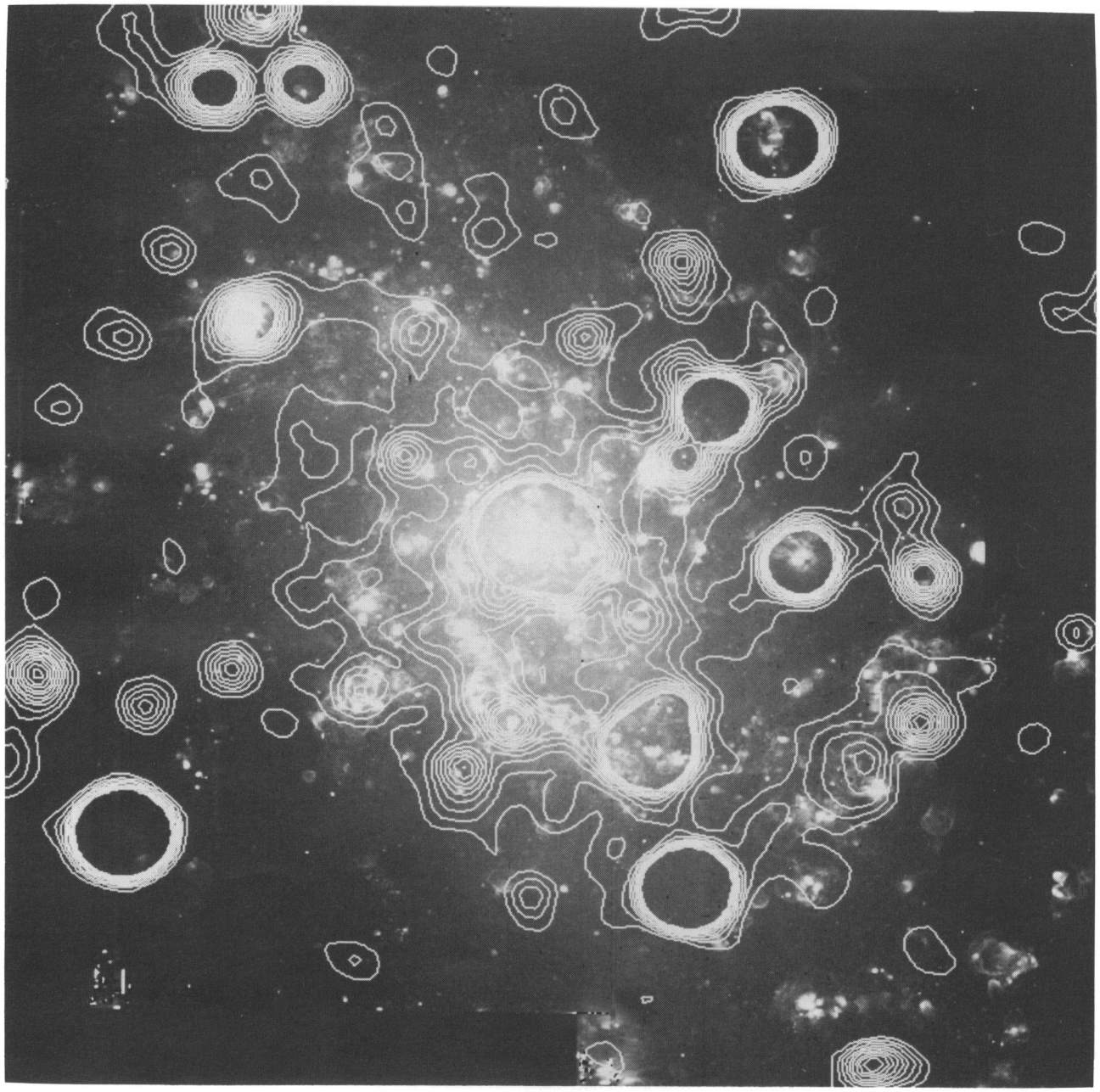

FIG. 2.—Central portion of the X-ray image superposed on an Hα mosaic of M33. The contours are identical to those presented in Fig. 1. The image is oriented so that north is up and east is to the left.

count rate and associated errors, and rejected any source detected at less than 3 σ.

A total of 50 sources survived this analysis, 37 of which lie within 15′ of the nucleus of M33. To obtain a qualitative description of the spectrum of each source, we calculated the hardness ratio $(H-S)/(H+S)$, where H and S are the net counts above and below 1 keV. Positions, count rates, luminosities, hardness ratios, and comments for these sources are presented in Table 1. The comments identify sources in our survey that had been previously identified in other X-ray surveys of M33, as well as possible identifications for the X-ray sources and an indication of whether the sources are variable. The luminosities quoted do not represent the results of detailed spectral fits to the data but rather assume a power-law spectrum $dF/dE \propto E^{-1}$ and log $N_H = 21$. With this assumption about the spectrum, the faintest source in our survey, which has a count rate of 4.9×10^{-4} s^{-1}, has a 0.1–2.4 keV luminosity of 10^{36} ergs s^{-1}. Other choices of a mean spectrum would produce only slightly different results. For example, if a bremsstrahlung spectrum with $kT = 0.25$ keV and log $N_H = 20.8$ was chosen, then the faintest source would have a luminosity of 6×10^{35} ergs s^{-1}.

There were 17 X-ray point sources identified in the M33 field sources as a result of the *Einstein* IPC and HRI surveys. (Two of the *Einstein* sources, X-9c [Christian & Schommer 1982] and X-11 [Long et al. 1981], were thought to be unassociated with M33.) Of the 17 *Einstein* sources, 14

TABLE 1

X-Ray Point Sources in M33

Source	R.A. (2000)	Decl. (2000)	Counts (in 10,000 s)	L_X[a] (10^{36} ergs s^{-1})	$(H-S)/(H+S)$[b]	Comments
1.....	1[h]30[m]44[s].9	30°33′00″.6	403.76 ± 16.62	81.73 ± 3.37	−0.44 ± 0.03	SAO 5478 (m_v = 10.2, G5)
2.....	1 31 39.5	30 37 28.7	73.71 ± 7.30	14.92 ± 1.48	−0.41 ± 0.08	Var (flare); HD 9269 (m_v = 8.3, K0 III)
3.....	1 31 44.9	30 22 13.1	161.01 ± 9.44	32.59 ± 1.91	−0.13 ± 0.06	Var; V-Tri (m_b = 10.9, A3)
4.....	1 32 29.8	30 36 21.3	10.37 ± 2.57	2.10 ± 0.52	0.00 ± 0.25	
5.....	1 32 53.1	30 38 20.0	39.00 ± 3.33	7.89 ± 0.67	−0.00 ± 0.09	X-1; RH 01; SNR 004+228
6.....	1 32 53.9	30 33 10.1	34.53 ± 3.53	6.99 ± 0.71	0.19 ± 0.11	X-2; RH 02
7.....	1 32 56.0	30 40 48.1	9.25 ± 2.06	1.87 ± 0.42	−0.07 ± 0.22	SNR 007+252(?); Var
8.....	1 33 01.9	30 31 54.3	16.73 ± 2.92	3.39 ± 0.59	−0.04 ± 0.17	
9.....	1 33 03.9	30 39 10.3	7.59 ± 1.96	1.54 ± 0.40	0.23 ± 0.28	
10.....	1 33 08.3	30 48 00.4	8.15 ± 1.85	1.65 ± 0.38	0.04 ± 0.23	
11.....	1 33 11.0	30 39 52.5	9.60 ± 2.04	1.94 ± 0.41	−0.41 ± 0.18	SNR 022+244
12.....	1 33 11.2	30 38 44.5	140.85 ± 5.73	28.51 ± 1.16	−0.52 ± 0.03	X-3; RH 04; SNR 022+233; NGC 592
13.....	1 33 14.8	30 53 28.5	449.71 ± 11.00	91.03 ± 2.23	0.35 ± 0.02	X-4; RH 05; SNR 136+396; B624
14.....	1 33 16.1	30 44 50.5	14.18 ± 2.73	2.87 ± 0.55	0.13 ± 0.20	IC 131
15.....	1 33 24.3	30 44 04.7	231.66 ± 7.41	46.90 ± 1.50	0.26 ± 0.03	X-5; RH 06
16.....	1 33 27.5	30 27 22.7	738.72 ± 13.27	149.54 ± 2.69	0.11 ± 0.02	X-6; RH 07
17.....	1 33 29.3	30 45 30.7	15.25 ± 2.41	3.09 ± 0.49	0.24 ± 0.17	RH 10
18.....	1 33 29.5	30 42 14.7	30.78 ± 3.18	6.23 ± 0.64	−0.50 ± 0.09	RH 08; SNR 042+270
19.....	1 33 29.7	30 49 20.7	19.38 ± 2.63	3.92 ± 0.53	−0.68 ± 0.10	RH 09; SNR 040+338
20.....	1 33 30.4	30 33 44.7	29.84 ± 3.17	6.04 ± 0.64	−0.63 ± 0.09	X-14; RH 11; SNR 042+182; B209
21.....	1 33 33.8	30 32 12.8	499.60 ± 10.74	101.13 ± 2.17	0.23 ± 0.02	X-7 (eclipsing binary); RH 12; Var; B203
22.....	1 33 35.2	30 36 38.8	11.15 ± 3.18	2.26 ± 0.64	0.21 ± 0.32	RH 13; SNR 047+211; B31
23.....	1 33 37.0	30 47 14.8	4.90 ± 1.60	0.99 ± 0.32	−0.24 ± 0.29	
24.....	1 33 40.9	30 39 00.8	16.41 ± 2.53	3.32 ± 0.51	−0.33 ± 0.14	RH 14; B38
25.....	1 33 43.1	30 46 26.8	13.85 ± 2.18	2.80 ± 0.44	−0.52 ± 0.12	
26.....	1 33 46.4	30 37 50.8	22.79 ± 3.11	4.61 ± 0.63	0.20 ± 0.14	RH 15
27.....	1 33 48.5	30 29 54.8	7.78 ± 2.35	1.58 ± 0.48	0.23 ± 0.34	
28.....	1 33 50.9	30 39 36.8	6163.40 ± 36.21	1247.65 ± 7.33	0.20 ± 0.01	X-8; RH 16; nucleus; SNR 100+241; B93
29.....	1 33 54.7	30 33 10.8	19.20 ± 2.80	3.89 ± 0.57	−0.59 ± 0.11	X-13; RH 17; SNR 106+178; B700
30.....	1 33 55.8	30 37 32.8	15.63 ± 2.85	3.16 ± 0.58	0.55 ± 0.22	
31.....	1 33 56.8	30 51 32.8	8.24 ± 2.21	1.67 ± 0.45	−0.25 ± 0.23	
32.....	1 33 58.2	30 50 08.8	9.86 ± 2.03	2.00 ± 0.41	0.24 ± 0.23	
33.....	1 34 01.1	30 31 40.8	17.95 ± 2.61	3.63 ± 0.53	0.25 ± 0.16	
34.....	1 34 07.8	30 46 34.8	7.03 ± 2.17	1.42 ± 0.44	−0.45 ± 0.24	
35.....	1 34 10.1	30 42 18.7	13.48 ± 2.35	2.73 ± 0.48	−0.67 ± 0.12	SNR 121+271
36.....	1 34 16.4	30 34 16.7	14.11 ± 2.54	2.86 ± 0.51	−0.69 ± 0.12	SNR 125+192; B713
37.....	1 34 25.4	30 37 32.5	7.81 ± 2.42	1.58 ± 0.49	−0.24 ± 0.27	
38.....	1 34 25.5	30 55 24.5	78.09 ± 5.12	15.81 ± 1.04	0.20 ± 0.07	X-9b; RH 21
39.....	1 34 27.7	30 32 56.5	5.71 ± 1.81	1.16 ± 0.37	−0.02 ± 0.31	
40.....	1 34 33.5	30 47 10.4	64.91 ± 5.00	13.14 ± 1.01	−0.47 ± 0.06	RH 22; NGC 604
41.....	1 34 35.8	30 34 54.3	19.29 ± 2.61	3.90 ± 0.53	0.31 ± 0.15	B717
42.....	1 34 38.7	30 55 10.3	68.93 ± 5.36	13.95 ± 1.09	0.02 ± 0.08	X-9a
43.....	1 34 45.2	30 49 16.1	18.60 ± 3.57	3.77 ± 0.72	−0.03 ± 0.19	
44.....	1 34 47.8	30 33 32.0	15.53 ± 2.51	3.14 ± 0.51	0.39 ± 0.18	
45.....	1 34 51.7	30 29 05.9	745.33 ± 13.99	150.88 ± 2.83	0.06 ± 0.02	X-10; RH 25
46.....	1 34 52.8	30 46 19.9	12.54 ± 3.48	2.54 ± 0.70	0.09 ± 0.29	
47.....	1 35 04.4	30 34 33.5	41.09 ± 4.28	8.32 ± 0.87	0.10 ± 0.11	RH 26
48.....	1 35 17.2	30 40 15.0	39.84 ± 4.71	8.07 ± 0.95	−0.86 ± 0.06	SAO 54806 (m_v = 9.3, G0)
49.....	1 35 51.6	30 44 47.3	266.93 ± 10.40	54.03 ± 2.10	−0.36 ± 0.04	X-11; Var (flare); HD 9687 (m_v = 8.2, K5)
50.....	1 36 12.9	30 48 54.0	180.20 ± 10.71	36.48 ± 2.17	−0.38 ± 0.05	

[a] The luminosity estimate is based upon a power-law spectrum $dF/dE \propto E^{-1}$ and log $N_H = 21$.

[b] The hardness ratios $(H-S)/(H+S)$ for each source are defined by net counts above and below 1 keV.

lie within 30″ of point sources in our survey and are likely to be the same object. The *Einstein* source X-9c lies in one of the regions partially obscured by the rib structure and was not included in our list. However, it can actually be seen in the flattened images at the position $1^h34^m38^s.3$, 30°57′52″ (J2000). The relatively bright HRI source X-12 is absent from our image; presumably, it is time variable. The source X-15, which lies about 90″ from the nucleus of M33, is not seen in our image. It was detected at less than 3 σ with the *Einstein* HRI, so its original identification might be questioned. In any event, it is quite close to the nucleus, and any diminution in the flux would have made it undetectable in our data. M33's X-ray appearance has not changed greatly in the decade between the *Einstein* and the *ROSAT* observations. The *ROSAT* luminosity function $N(>L)$ closely resembles the luminosity function obtained from the *Einstein* sources.

Schulman & Bregman (1995) detected 27 X-ray sources within 17.5 of the nucleus in their *ROSAT* HRI survey of M33. A comparison between the PSPC source list and the HRI source list reveals that 20 of the 27 HRI sources lie within 20″ of a PSPC source. As might be expected, the sources that do not overlap are those that are faint. All of the 17 sources detected with a signal-to-noise ratio (S/N) ≥ 4 in the HRI are in the PSPC list. However, only three of the 10 sources with $3 < \mathrm{S/N} < 4$ are in the PSPC list. Schulman & Bregman estimate that only one of the sources in their list is due to a random fluctuation in the background. We have checked to see whether source confusion could account for the absence of these sources in our survey. With the exception of RH 23, which is located 1.2 from PSPC source No. 40 (identified with NGC 604), the missing HRI sources are in relatively unconfused regions of the PSPC field. The PSPC and HRI observing times were comparable, and the PSPC is somewhat more sensitive than the HRI, which seems to suggest that the HRI sources missed in the PSPC survey must be time variable or that Schulman & Bregman have slightly overestimated the significance of the detections of the faintest sources in their survey. There are additional *ROSAT* HRI observations of M33, so it should be possible to determine which of these possibilities is correct.

The faintest source in our sample has an observed flux of 6×10^{-15} ergs cm^{-2} s^{-1} in the energy range 0.1–2.4 keV, or 2.4×10^{-15} ergs cm^{-2} s^{-1} in the range 0.4–2 keV, given our assumptions about the spectrum. Hasinger et al. (1994) have used source counts in the direction of Lockman's hole, a line of sight with very low column density to calculate a log N–log S curve for (extragalactic) sources as observed with *ROSAT*. They find that there are several hundred sources per square degree at a flux limit of 10^{-14} ergs cm^{-2} s^{-1}. It is important to remember, however, that Hasinger et al. have effectively calculated the log N–log S curve once absorption has been removed. An observed flux of 2.4×10^{-15} ergs cm^{-2} s^{-1} (0.4–2.0 keV) corresponds to an incident flux of 8.4×10^{-14} ergs cm^{-2} s^{-1} if Galactic absorption of 6×10^{20} cm^{-2} (Stark et al. 1992) is removed, or 1.18×10^{-13} ergs cm^{-2} s^{-1} if a total absorption of 10^{21} cm^{-2} (Newton 1980) is assumed. At these limits, there are expected to be 3–5 interlopers per square degree. As a result, at most one interloper is expected in the inner 15′ of the M33 field.

The nuclear source contributes about 70% of the luminosity of the galaxy. In the PSPC energy range, the X-ray spectrum is hard, similar to that expected either from (a collection of) binary X-ray sources or from an active galactic nucleus. We have fitted the pulse-height distribution (PI bins 3–34) of the nucleus to bremsstrahlung and power-law models using the spectral routines contained in PROS. The PSPC data are well fitted ($\chi^2_{\min} = 31.3$ with 30 degrees of freedom) in terms of a bremsstrahlung model with $kT = 3.2$ keV and log $N_{\mathrm{H}} = 21.06$. The 99% confidence contours ($\chi^2_{\min} + 9.21$) imply that 2.4 keV $< kT <$ 4.6 keV and $21.01 < \log N_{\mathrm{H}} < 21.13$. The power-law fits ($\chi^2_{\min} = 40.8$) yield an energy index α of 0.74 and a log N_{H} of 21.13, and limits of $0.56 < \alpha < 0.97$ and $21.06 < \log N_{\mathrm{H}} < 21.24$. The 0.1–2.4 keV luminosity implied by the best-fit bremsstrahlung spectrum is 1.1×10^{39} ergs s^{-1}. Higher spectral resolution data taken with the *Advanced Satellite for Cosmology and Astrophysics* (*ASCA*) over a wider energy range (0.5–10 keV) by Takano et al. (1994) show that the spectrum of the nuclear source is well fitted by a flat power law ($\alpha = 0.7$), in agreement with the PSPC value, but that the spectrum is exponentially cut off above 2 keV. This means that the spectrum of the nuclear source is significantly softer than spectra of normal active galactic nuclei. Takano et al. go on to fit the *ASCA* data to a multicolor disk plus power-law model that is typical of the X-ray spectra of the black hole X-ray transients in outburst. The value of N_{H} derived from the PSPC data is roughly consistent with that expected to the center of the galaxy, based on 21 cm measurements of N_{H} along the line of sight to the nucleus. Analogous fits to the *Einstein* IPC data carried out by Trinchieri et al. (1988) yielded similar values of kT and α, but larger N_{H} ($\sim 5 \times 10^{21}$ cm^{-2}), and were used to argue that the nuclear source was intrinsically absorbed.

The 0.2–4.0 keV luminosity estimates made by Trinchieri et al. (1988), assuming a "fiducial" bremsstrahlung spectrum with kT of 5 keV and N_{H} of 6×10^{20} cm^{-2}, from the *Einstein* HRI and IPC observations of the nuclear source were 8.1×10^{38} and 9.4×10^{38} ergs s^{-1}, respectively. For this spectral shape, the PSPC observations suggest a 0.2–4.0 keV luminosity of 8.8×10^{38} ergs s^{-1}. This difference is quite modest, given the fact that the data were acquired from two different instruments with different bandpasses, and indicates that the source has not changed significantly since the *Einstein* observations 10 years earlier.

The nature of the nuclear source or sources is not well understood. Possibilities include a superluminous galactic X-ray source, a miniquasar, or a collection of otherwise normal galactic X-ray binaries. We do observe temporal variations in M33 X-8 in these PSPC and accompanying HRI observations of M33. A study of the temporal variability of M33 X-8 in these PSPC and accompanying HRI observations of M33 is currently in progress and will be the subject of a future paper.

Other sources, including X-7, are clearly variable in our PSPC data. An analysis of the temporal properties of the sources is beyond the scope of this paper, but we have done a preliminary analysis both by calculating count rates for the three observing intervals and by plotting count rates of all the sources as a function of time. Sources that are clearly variable have been noted as "Var" in Table 1.

There appear to be no supersoft sources, objects with blackbody temperatures of order 30 eV, and bolometric luminosities of order 10^{38} ergs s^{-1} (see, e.g., Hasinger 1994) in our point-source sample. Specifically, there are no objects that have hardness ratios $(H' - S')/(H' + S') < -0.8$, where

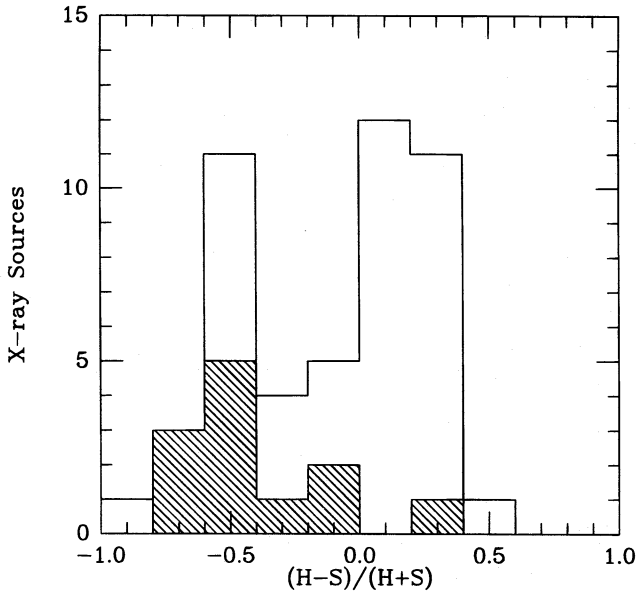

FIG. 3.—Hardness ratios $(H-S)/(H+S)$ for the sources in M33, where H and S are defined as the number of counts above and below 1 keV. Sources less than 30″ from confirmed SNRs are crosshatched.

H' and S' are the 0.5–2.0 and 0.1–0.4 keV count rates, respectively. For example, the object (48) that has the most negative hardness ratio using our pulse-height boundaries has a ratio of − 0.14 as defined here. If supersoft sources do exist in our sample, they must lie behind considerable absorption. Assuming that a typical supersoft source had a blackbody spectrum with kT of 50 eV and that absorption along the line of sight corresponded to log $N_{\rm H}$ of 20.8, then the luminosity limit for our survey is about 3×10^{36} ergs s^{-1}. There were 15 supersoft sources identified by this procedure in the M31 sample. If the ratio of supersoft to total sources were similar in M33, one might have expected to find two supersoft sources in M33, so the absence of any such sources is not especially surprising.

3.2. *Supernova Remnants*

There are now 98 emission nebulae in M33 that are thought to be SNRs on the basis of optical interference filter imagery and (in most cases) follow-up optical spectroscopy and VLA radio observations (Long et al. 1990; Smith et al. 1993; Gordon 1995; Gordon et al. 1996). Of these SNRs, 88 lie within 15′ of the nucleus of M33, where the X-ray imaging is of high quality. Of the 37 X-ray sources within this region, 10 (12) lie within 20″ (30″) of known SNRs. If we assume that the 37 X-ray sources and the 88 SNRs are randomly distributed within 15′ of the nucleus, then less than 2 (4) chance coincidences would be expected.

Figure 3 is a histogram of the number of sources as a function of the hardness ratio $(H-S)/(H+S)$ (as defined by our standard pulse-height boundary at 1 keV). The sources that lie near the SNRs, which are shown as the "hatched" regions in the figure, are clearly softer than the bulk of the sources. This argues strongly that most of the X-ray sources that are spatially coincident with known SNRs are indeed SNRs. It also suggests that some of the other soft sources are likely to be SNRs that have not been identified in the optical surveys and that this hardness ratio could be used to identify SNRs in *ROSAT* PSPC surveys of other nearby galaxies.

Boulesteix et al. (1974) list 176 bright (EM > 1600 cm^{-6} pc) emission nebulae in M33. The vast majority of these objects are H II regions, although some are SNRs (and others have SNRs buried in them). Boulesteix et al., using Hα imagery only, could not distinguish between these possibilities. H II regions themselves are weak X-ray emitters. However, they might be expected to contain sources such as massive X-ray binaries that would produce strong X-ray emission. Therefore, we compared the Boulesteix et al. list with our X-ray sample. We found 8 (11) X-ray objects that lie within 20″ (30″) of emission-line nebulae. Of these, only 3 (6) are expected by chance. Of the coincidences, four X-ray objects, Nos. 39, 104, 105, and 106, are also found in the SNR sample. Object No. 39 has been discussed in detail by Gordon et al. (1994) and is a SNR buried in the H II region NGC 592. Assuming that the other three coincidences are actually SNRs, then there are only 4 (7) X-ray sources that are coincident with H II regions (lacking SNRs). This is about what one would expect by chance, and hence there is no evidence for a population of sources (other than SNRs) associated with bright H II regions in M33.

3.3. *Diffuse Emission*

Diffuse soft X-ray emission from the galaxy is detected. The vignetting-corrected azimuthally averaged 0.4–2.4 keV surface brightness distribution with and without the resolved point sources is shown as a function of radius in Figure 4. The azimuthally averaged diffuse flux declines between 2′ and 10′ from the nucleus, from 6×10^{-4} s^{-1} arcmin^{-2} to about 10^{-4} s^{-1} arcmin^{-2}. There is no evidence for emission more than 15′, or 3 kpc, from the nucleus. Summing the diffuse flux in each radial bin, allowing for the regions dominated by point sources, and using the bins between 25′ and 37.5 from the nucleus to estimate the cosmic (and any residual detector) background in the neighborhood of M33, the "diffuse" flux produces 0.12 s^{-1}. This is 11% of the total X-ray count rate, and 31% of the flux attributed to point sources other than the nucleus. The $D(25)$ diameter of M33

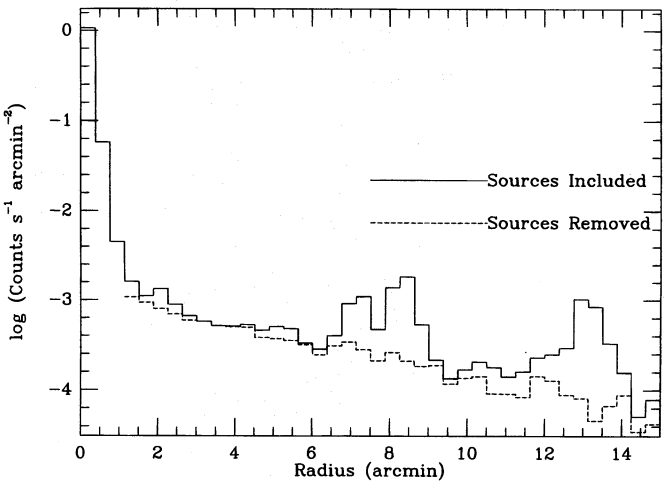

FIG. 4.—The azimuthally averaged (0.4–2.4 keV) X-ray surface brightness of M33 as a function of radius. The solid line includes both the point source and the diffuse components to the emission, while the dashed line excludes the flux from point sources.

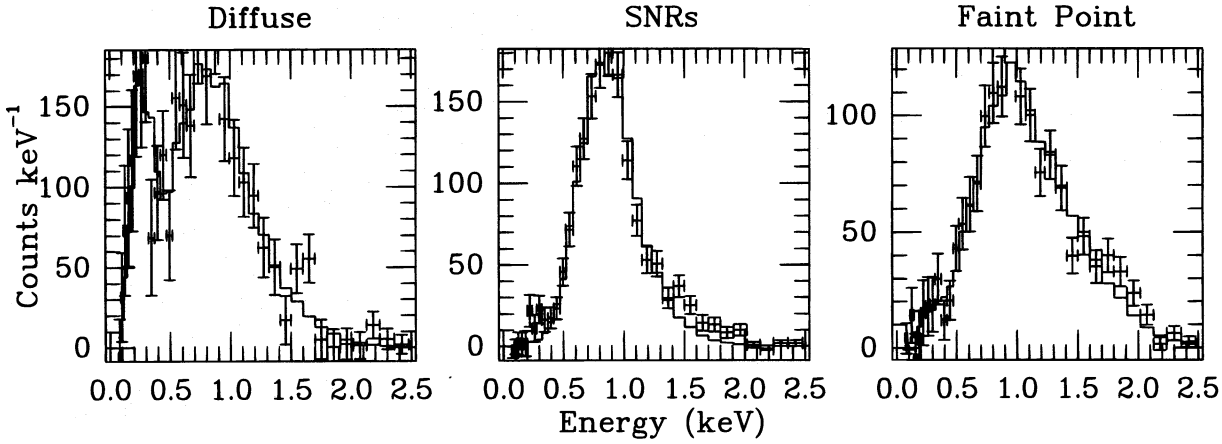

FIG. 5.—Spectrum of the diffuse flux from M33 compared with that of the sources identified with SNRs and with the fainter point sources not coincident with SNRs. There is a significant 0.25 keV component in the diffuse emission and a hard X-ray tail in the summed spectrum of faint point sources. These differences are reflected in the fits to the spectra that are shown as the solid histograms.

is 71′, or 15 kpc, so the detectable diffuse emission is confined to the inner 40% (in radius) of the galaxy.

We have also constructed azimuthally averaged surface brightness profiles in the 0.25 keV (R1 + R2), 0.75 keV (R4 + R5), and 1.5 keV (R6 + R7) bands defined by SMBM. Each band shows excess emission out to ~15′ from the nucleus, as was the case for our broadband profile. However, the azimuthal distributions in the bands differ. The southern spiral arm of the galaxy is quite prominent at 0.75 and 1.5 keV, but almost absent at 0.25 keV, suggesting that there is a significant Population I component to the harder flux.

In an attempt to characterize the diffuse emission from M33, we extracted a spectrum from the region between 4′ and 10′ from the nucleus, using the background annulus described above and eliminating identified point sources from both the source and the background regions. For comparison, we also extracted and summed the spectra of all the faint sources (≤ 100 excess counts) in the M33 image and all the sources identified with SNRs. A comparison of the spectra is shown in Figure 5. For the diffuse X-ray emission, thermal bremsstrahlung fits yield log $N_{\rm H} = 20.6$ and $kT = 0.4$ keV. For the sum of the faint sources, fits yield log $N_{\rm H} = 20.8$ and $kT = 1.1$ keV. Trinchieri et al. (1988) had previously pointed out that the diffuse emission in M33 is softer than the spectra of the bright sources; the *ROSAT* observations show that it is softer than most of the faint point sources as well. The spectrum of the diffuse component is also quite different from the sources we have identified with SNRs, which, for thermal bremsstrahlung fits, yield very high column densities and very low temperatures. This argues strongly that the diffuse X-ray emission in M33 is not simply due to faint, unresolved X-ray binaries or SNRs, and suggests to us that there is a significant hot interstellar gas contribution to the diffuse emission, analogous to the 0.25 keV background in our Galaxy.

4. CONCLUSIONS

Our *ROSAT* observation of M33 has allowed us to characterize the X-ray emission to this nearby galaxy to a lower surface brightness limit than was possible with earlier data. Most of the sources detected with *Einstein* a decade before are still visible, including the X-ray nucleus of M33. Most of the *Einstein* sources were luminous X-ray binaries. The *ROSAT* observations reveal a relatively large, new population of X-ray SNRs. Although the observations have yielded additional point sources, they have not resolved the diffuse emission observed with *Einstein* into point sources. Diffuse emission, characterized by a spectrum softer than that of the point sources, contributes approximately 31% of the nonnuclear soft X-ray flux from the galaxy.

This work has been supported by NASA grant NAG 5-1539 to the STScI. P. A. C. acknowledges travel support from SERC grant GR/H69120, and the hospitality of the STScI. We also appreciate referee Alfonso Collura's careful reading of the original manuscript.

REFERENCES

Boulesteix, J., Courtès, G., Laval, A., Monnet, G., & Petit, H. 1974, A&A, 37, 33
Christian, C. A., & Schommer, R. A. 1982, ApJ, 253, L13
de Vaucouleurs, G. 1978, ApJ, 224, 710
de Vaucouleurs, G., & Leach, R. W. 1981, PASP, 93, 190
Gordon, S. M. 1995, Ph.D. thesis, Univ. New Mexico
Gordon, S. M., Kirshner, R. P., Duric, N., & Long, K. S. 1994, ApJ, 418, 743
Gordon, S. M., Kirshner, R. P., Duric, N., Long, K. S., Blair, W. P., & Smith, R. C. 1996, in preparation
Hasinger, G. 1994, in AIP Conf. Proc. 308, The Evolution of X-Ray Binaries, ed. S. S. Holt & C. S. Day (New York: AIP), 611
Hasinger, G., Burg, R., Giacconi, R. Hartner, G., Schmidt, M., Trümper, J., & Zamorani, G. 1994, A&A, 291, 348
Long, K. S., Blair, W. P., Kirshner, R. P., & Winkler, P. F. 1990, ApJS, 72, 61
Long, K. S., D'Odorico, S., Charles, P. A., & Dopita, M. A. 1981, ApJ, 246, L61
Markert, T. H., & Rallis, A. D. 1983, ApJ, 275, 571
Newton, K. 1980, MNRAS, 190, 689
Peres, G., Reale, F., Collura, A., & Fabbiano, G. 1989, ApJ, 336, 140
Pfeffermann, E., et al. 1986, Proc. SPIE, 733, 519
Searle, L. 1971, ApJ, 168, 327
Schulman, E., & Bregman, J. N. 1995, ApJ, 441, 568

Schulman E., Bregman, J. N., Collura, A., Reale F., & Peres, G. 1993, ApJ, 418, L67
———. 1994, ApJ, 426, L55
Smith, R. C., Kirshner, R. P., Blair, W. P., Long, K. S., & Winkler, P. F. 1993, ApJ, 407, 564
Snowden, S. L. 1994, Cookbook for Analysis Procedures for *ROSAT* XRT/PSPC Observations of Extended Objects and the Diffuse Background (Greenbelt: NASA/GSFC)
Snowden, S., McCammon, D., Burrows, D. N., & Mendenhall, J. A. 1994, ApJ, 424, 714 (SMBM)
Stark, A. A., Gammie, C. F., Wilson, R. W., Balley, J., Linke, R. A., Heiles, C., & Hurwitz, M. 1992, ApJS, 79, 77
Takano, M., Mitsuda, K., Fukazawa, Y., & Nakase, F. 1994, ApJ, 436, L47
Trinchieri, G., Fabbiano, G., & Peres, G. 1988, ApJ, 325, 531
Trümper, J. 1983, Adv. Space Res., 2(4), 241